Theoretical study on isomerization of α-acids: A DFT calculation

AUTHOR(S):

Kimura, Minami; Ito, Tadashi; Sato, Hirofumi; Higashi, Masahiro

CITATION:

Kimura, Minami ...[et al]. Theoretical study on isomerization of α-acids: A DFT calculation. Food Chemistry 2021, 364: 130418.

ISSUE DATE:

2021-12

URL:

http://hdl.handle.net/2433/285541

Theoretical Study on Isomerization of α-Acids: A DFT Calculation

Minami Kimura[a], Tadashi Ito[b,1], Hirofumi Sato[a,c,d], Masahiro Higashi[a,c]*

[a]Department of Molecular Engineering, Graduate School of Engineering, Kyoto University, Kyoto 615-8510, Japan

[b]Department of Chemistry, Biology and Marine Science, University of the Ryukyus, 1 Senbaru, Nishihara, Okinawa 903-0213, Japan

[c]Elements Strategy Initiative for Catalysts and Batteries (ESICB), Kyoto University, Kyoto 615-8520, Japan

[d]Fukui Institute for Fundamental Chemistry, Kyoto University, Kyoto 606-8103, Japan

*Corresponding Author

E-mail address: higashi@moleng.kyoto-u.ac.jp

[1]Present address:
Ushitora Co. Ltd., Ushitora brewery, 142-3, Sasahara, Shimotsuke, Tochigi 329-0402, Japan

ABSTRACT:

The α-acids contained in hops are one of the ingredients of beer. The isomerization of α-acids produces iso-α-acids, the main source of bitterness in beer. In this study, the isomerization mechanism of the α-acid, cohumulone, was elucidated by using density functional theory in conjunction with the polarizable continuum model or 3D-RISM integral equation theory of liquids. The calculated reaction diagram is consistent with experimental results; the activation free energy difference between the *cis* and *trans* isomers is in good agreement with the experimental estimate. The activation energy difference results from solvation energy. Additionally, a calculation of NMR chemical shifts showed that the proton position of isocohumulone is different from that proposed previously. The effect of Mg^{2+} cation on the isomerization was also investigated. Both the activation and reaction free energy are stabilized by the presence of Mg^{2+}, which is consistent with experimental results. Water solvation reduces the activation free energy.

KEYWORDS: α-acid; iso-α-acid; isomerization; cohumulone; metal cation effect; solvent effect

1. Introduction

Hops (*Humulus lupulus* L.) have been cultivated around the world, such as in Europe, North America, Australia, and Asia (Delyser & Kasper, 1994). Among the many uses of hops, its biological activities, such as its anti-inflammatory and antioxidant properties, have been

exploited for medical purposes (Zanoli & Zavatti, 2008). Hops are a well-known raw material for beer and are one of the four essential ingredients of beer: barley malt, brewing water, yeast, and hops (Denis De Keukeleire, 2000). Hops impart a characteristic aroma and taste to beer, especially bitterness (Schönberger & Kostelecky, 2011).

The important chemical compounds in hop flowers are α-acids. Unique side chains are found in some types of α-acids, such as humulone, cohumulone, and adhumulone (Scheme 1). α-acids do not have a bitter taste. Heating α-acids results in thermal isomerization via an acyloin-type ring contraction. The isomerization products are iso-α-acids, the main bitter-tasting components of beer. These iso-α-acids have *cis*/*trans* isomers (Scheme 1) (Jaskula-Goiris et al., 2010).

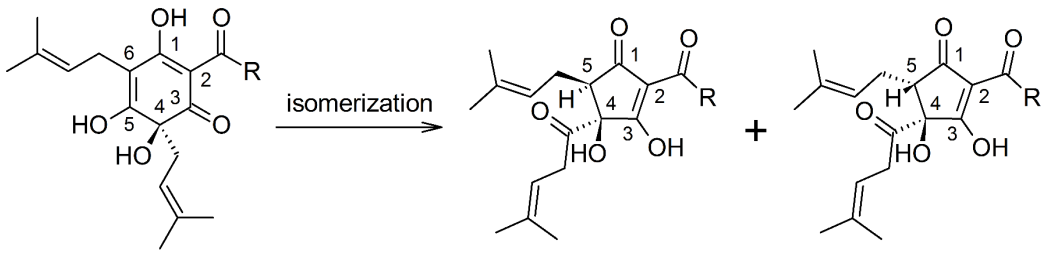

Scheme 1. Isomerization of α-acids to *cis*/*trans*-iso-α-acids: cohumulone, humulone, and adhumulone correspond to R= isopropyl, 2-methylpropyl, and 1-methylethyl, respectively

Many experimental studies have been performed to elucidate the isomerization mechanism of α-acids (Askew, 1964; Jaskula et al., 2008; Malowicki & Shellhammer, 2005;

Ocvirk & Košir, 2020; Verzele & van Boven, 1971). For example, the isomerization rate was measured in an aqueous buffer at pH 5.2 and 90–130°C (Malowicki & Shellhammer, 2005). The isomerization rate was found to be first order in the α-acid concentration, and the activation energy for the overall *cis* and *trans* isomerization was found to be 23.6 kcal/mol. Jaskula et al. (Jaskula et al., 2008) subsequently measured the *cis* and *trans* isomerization rates and proposed the difference in reaction profiles between the *cis* and *trans* isomers. The activation energy for the isomerization of *cis*-iso-α-acids is several kcal/mol higher than that of *trans*-iso-α-acids. There is a 3.4-kcal/mol difference in the activation energies of *cis* and *trans* cohumulone. By contrast, *cis*-iso-α-acids have a lower reaction energy than *trans*-iso-α-acids. The aforementioned studies determined the kinetics and thermodynamics of isomerization. However, the molecular mechanism for isomerization has not been elucidated.

Many experimental studies on the structural analysis of iso-α-acids have also been carried out (D. De Keukeleire & Verzele, 1971; Hoek et al., 2001; Khatib et al., 2007; Urban et al., 2013; Verzele & van Boven, 1971). The absolute configuration of *cis*-isohumulone was first determined as (4*R*, 5*S*) by Horeau's method in 1971 (D. De Keukeleire & Verzele, 1971; Verzele & van Boven, 1971). This structure has been used for over 40 years, including to assign ^{13}C and ^{1}H NMR chemical shifts (Hoek et al., 2001; Khatib et al., 2007). In 2013, the absolute configuration of *cis*-iso-α-acids was redetermined as (4*S*, 5*R*) by X-ray crystallography (Urban et al., 2013). These measurements were used to identify almost the entire molecular configuration. However, it is still difficult to accurately determine the positions of hydroxyl

protons using these measurements. An alternative molecular configuration, 1-OH-PRD (shown below), to the traditional configuration, 3-OH-PRD, is possible.

Isomerization yields are affected by various factors, such as the pH and metal cations (Jaskula et al., 2010; Steenackers et al., 2015). Several metal cations have long been known to affect isomerization (Lance et al., 1975). In particular, the acceleration effect of Mg^{2+} on isomerization has been well studied (Köller, 1969). Isomerization with the addition of magnesium oxide, MgO, at ambient temperature produces high yields with no side products. Increasing the quantity of MgO added has been shown to increase the yield over fewer days of reaction (Kostrzewa et al., 2016). This effect of Mg^{2+} on isomerization could be attributed to complex formation between an α-acid and a Mg^{2+} cation, because α-acids have a 1,4-diketone structure. This O-Mg-O structure is also found in the RNA folding, where Mg^{2+} cation is more suitable than other cations such as Na^{+} and Ca^{2+} for its size and charge density (Petrov et al., 2011). However, Wietstock et al. recently carried out UV-VIS spectroscopy on α-acid and metal cation mixtures and proposed no complexation between α-acids and Mg^{2+} (Wietstock et al., 2016). The spectrum of equimolar mixtures of α-acids and Fe^{2+} was found to differ from that of α-acids alone, indicating complexation between α-acids and Fe^{2+}, whereas equimolar mixtures of α-acids and Mg^{2+} exhibited a similar spectrum to that of α-acids alone. Thus, the mechanism for the effect of Mg^{2+} on isomerization remains controversial.

The purposes of this study are to theoretically examine the isomerization mechanism of cohumulone (R=isopropyl), the hydroxyl proton position for isocohumulone, and the effect of Mg^{2+} addition on isomerization. There are some theoretical studies on the chemical reaction

of ingredients of foods and beverages (D. Milenković et al., 2018; D. A. Milenković et al., 2020; Tošović et al., 2017). However, to the best of our knowledge, no theoretical studies on hop α-acid isomerization have been performed to date. First, the transition state structure and the activation free energy are analyzed to elucidate the isomerization mechanism. Next, the position of the hydroxyl proton is determined by comparing calculated and experimentally measured NMR chemical shifts. Finally, the activation free energy of isomerization with Mg^{2+} is decomposed into several components to identify the main effect of the metal cation on the stability of isomerization.

2. Material and methods

We used density functional theory (DFT) in conjunction with the polarizable continuum model (PCM) or three-dimensional reference interaction site model (3D-RISM) integral equation theory (Beglov & Roux, 1997; Kovalenko & Hirata, 1998) to investigate the isomerization mechanism of cohumulone, the NMR spectra of cohumulone and isocohumulone, and the absorption spectra of cohumulone and complexes between cohumulone and metal cations. The combination of quantum chemical method and 3D-RISM theory is referred to as 3D-RISM-SCF method (Sato et al., 2000; Yoshida et al., 2011; Yoshida & Hirata, 2006), which enables us to obtain molecular solvation structure around a solute. The geometries of the reactants, intermediates, transition states, and products in solution were optimized at the B3LYP-GD3(BJ)/6-31+G(d,p) level with the SMD solvent model (Marenich et al., 2009). Notably, the dispersion correction, such as the D3 version of Grimme's dispersion

with Becke-Johnson damping, GD3(BJ) (Grimme et al., 2011), is needed to reproduce the experimental reaction profile. To match the experimental conditions, the reaction profile and absorption spectra were calculated in aqueous solution, whereas the NMR chemical shifts were calculated in chloroform solution. Frequency calculations were used to obtain thermal corrections to the Gibbs free energies at 25°C (Ochterski & Ph, 2000). Truhlar's quasiharmonic approximation was adopted for the free energy calculations to correct for the spurious overestimation of vibrational entropies introduced by treating low-frequency vibrational modes as harmonic oscillators. This uses the same usual harmonic oscillator approximation in the calculations of the vibrational partition functions, except that all of the vibrational frequencies that are lower than 100 cm^{-1} are set equal to 100 cm^{-1}(Lam & Houk, 2014; Ribeiro et al., 2011). The same geometries optimized at SMD-B3LYP-GD3(BJ)/6-31+G(d,p) level were used for 3D-RISM-SCF calculations. The Kovalenko-Hirata closure is employed to solve the 3D-RISM calculation. The Lennard-Jones parameters for solutes were taken from the general AMBER force field (GAFF) (Wang et al., 2004). The simple point charge (SPC) (Berendsen et al., 1981) model with modified hydrogen parameters (σ = 1.0 Å and ε = 0.056 kcal/mol) was used for water solvent. The grid points in the 3D-RISM-SCF calculations were 128×128×128 with a spacing of 0.5 Å. The gauge-independent atomic orbital (GIAO) (Ditchfield, 1974) method and time-dependent DFT (TDDFT) were employed to calculate the NMR and absorption spectra, respectively. NMR spectra are calculated by using the SMD model because the solvent effect of non-polar chloroform is considered to be small. All the calculations were

performed using Gaussian 16 (Frisch et al., 2016), and a modified version of GAMESS (Schmidt et al., 1993) where the 3D-RISM-SCF method has been implemented (Yoshida & Hirata, 2006).

3. Results and Discussion

3-1. Isomerization reaction profile

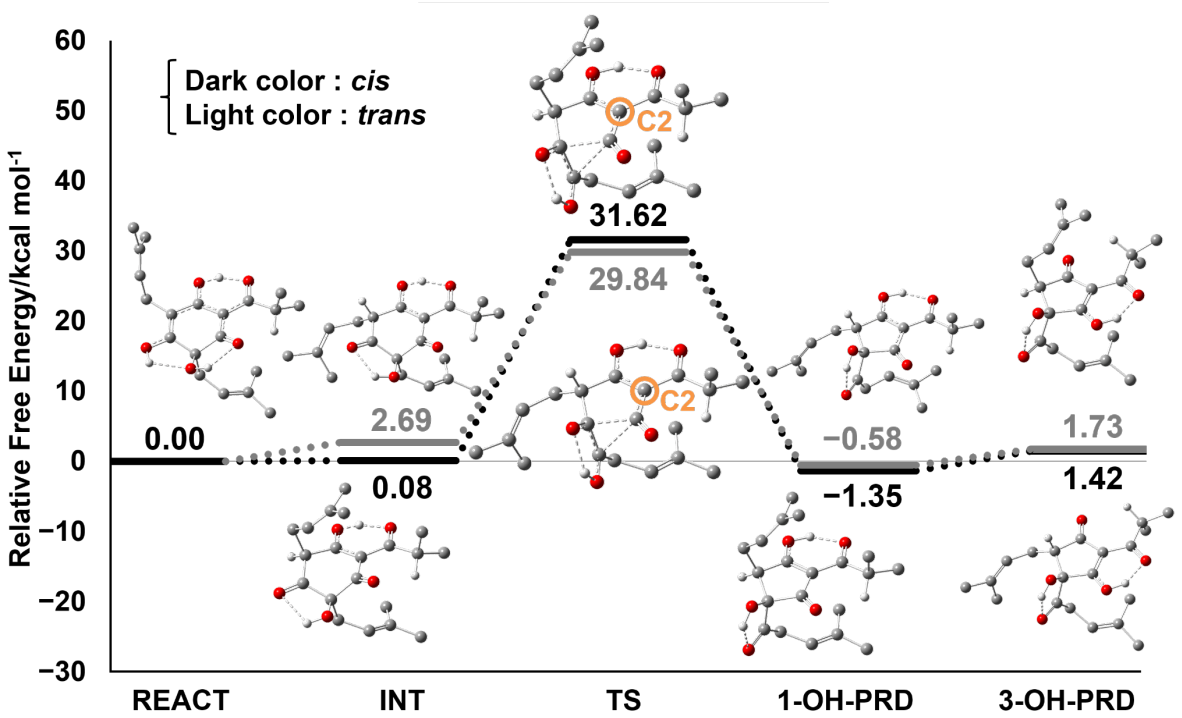

Figure 1. Cohumulone isomerization reaction profile

We first analyzed the mechanism of cohumulone isomerization. Following previous studies, (D. De Keukeleire & Verzele, 1971; Steenackers et al., 2015) the reaction path in Scheme S1 (Supplementary Materials) was assumed. In the first step, keto-enol tautomerization generates the *cis* and *trans* intermediates, INT_{cis} and INT_{trans}, from the reactant

145 cohumulone (REACT). Next, INT_{cis} and INT_{trans} pass through two transition states, TS_{cis} and
146 TS_{trans}, and are converted into two products that both have a hydroxy group at the C1 position,
147 1-OH-$PRD_{cis/trans}$. Finally, the equilibrium between 1-OH-$PRD_{cis/trans}$ and 3-OH-$PRD_{cis/trans}$ with
148 a hydroxy group at the C3 position is investigated. Note that 3-OH-$PRD_{cis/trans}$ are traditionally
149 regarded as the structures of *cis/trans* isocohumulone (Urban et al., 2013). It is also noted that
150 no direct involvement of water in the reaction was assumed because intramolecular ring
151 contraction and proton transfer are found to proceed at the TSs in a concerted manner.
152 The reaction profile calculated with the 3D-RISM-SCF method is shown in Figure 1.
153 Both INT_{cis} and INT_{trans} are unstable compared with REACT by ~3 kcal/mol. The activation free
154 energy of TS_{cis} (31.62 kcal/mol) is higher than that of TS_{trans} (29.84 kcal/mol), whereas the *cis*
155 products, 1-OH-PRD_{cis} and 3-OH-PRD_{cis}, have lower reaction free energies (−1.35 and 1.42
156 kcal/mol, respectively) than the *trans* products, 1-OH-PRD_{trans} and 3-OH-PRD_{trans} (−0.58 and
157 1.73 kcal/mol, respectively). These calculated results are consistent with experimental results
158 (Jaskula et al., 2008). The calculated activation free energy difference of 1.78 kcal/mol between
159 the *cis* and *trans* products is in good agreement with the experimental value of 3.4 kcal/mol
160 (Malowicki & Shellhammer, 2005). Furthermore, 1-OH-PRDs are found to be more stable than
161 3-OH-PRDs, which suggests that 1-OH-PRDs are more realistic candidates for the structure
162 of isocohumulone (see discussion below).
163

164 **3-2. Analysis of TS*cis/trans***

165 The difference in the activation free energies of the *cis* and *trans* products was analyzed.
166 We decomposed the free energy difference between the TS*cis* and TS*trans*, ΔG = 1.78 kcal/mol,
167 into three contributions, the structural energy difference in the gas phase ΔE_{gas}, the solvation
168 free energy difference $\Delta \mu_{\mathrm{sol}}$, and thermal free energy difference $\Delta G_{\mathrm{thermal}}$:

169 $$\Delta G = \Delta E_{\mathrm{gas}} + \Delta \mu_{\mathrm{sol}} + \Delta G_{\mathrm{thermal}} \quad (1)$$

170 where $\Delta E_{\mathrm{gas}} = E_{\mathrm{gas}}(\mathrm{TS}_{cis}) - E_{\mathrm{gas}}(\mathrm{TS}_{trans})$, and $\Delta \mu_{\mathrm{sol}}$, and $\Delta G_{\mathrm{thermal}}$ are defined analogously. ΔE_{gas}
171 is calculated to be –4.71 kcal/mol, indicating that TS*cis* has lower structural energy than TS*trans*.
172 On the other hand, TS*trans* has lower solvation free energy than TS*cis*, $\Delta \mu_{\mathrm{sol}}$ = 6.33 kcal/mol.
173 $\Delta G_{\mathrm{thermal}}$ is found to be as small as 0.16 kcal/mol. These results demonstrate that solvation plays
174 a major role in the stabilization of TS*trans*. Notably, the sophisticated 3D-RISM-SCF method was
175 needed for the proper description of solvation. The SMD solvation model failed to reproduce
176 the experimental result; the free energy of TS*trans* (28.43 kcal/mol) calculated with the SMD
177 model is similar to that of TS*cis* (28.40 kcal/mol).

178 Further analysis decomposing the solvation free energy into each atom contribution
179 showed that the main reason for the difference is the C2 atom, the center of the β-triketo
180 system. TS*cis* has low structural energy due to the interaction between the C2 atom and side
181 chain whereas TS*trans* has low solvation free energy due to the strong solvation of the C2 atom.
182 The importance of the stabilization of the β-triketo system for the isomerization was suggested
183 in the previous study (Jaskula-Goiris et al., 2010).

184

185 **3-3. Proton position**

186 Experimental studies have reported 3-OH-PRD as the isomerization end product
187 (Urban et al., 2013). However, the calculated reaction profile showed that 1-OH-PRD is more
188 stable than 3-OH-PRD (Figure 1). We analyzed the proton position in more detail by
189 calculating the ^{13}C and ^{1}H NMR chemical shifts of REACT, PRD$_{cis}$, and PRD$_{trans}$ for comparison
190 with experimental data (Hoek et al., 2001; Khatib et al., 2007). Although direct comparison is
191 precluded by the unavailability of NMR data for hydroxyl protons, a useful comparison can be
192 made for NMR data for ^{13}C and other protons. The atomic numbering of REACT, PRD$_{cis}$, and
193 PRD$_{trans}$ is shown in Figure S1.

194 First, the NMR spectra of REACT were used as a reference. The calculated and
195 experimental NMR chemical shifts of REACT and the correlation between these results are
196 shown in Table S1 and Figure 2. Reasonably good correlations are obtained for both ^{13}C and
197 ^{1}H, with coefficients of determination, R^2, of 0.9980 and 0.9947, respectively. This result
198 validates our NMR calculation.

199 Figure 2 shows the correlations between the experimental and calculated NMR
200 chemical shifts for 3-OH-PRDs (the proposed isocohumulone structure) and 1-OH-PRDs (the
201 lower free energy). The calculated and experimental NMR chemical shifts of 3-OH-PRDs and
202 1-OH-PRDs are summarized in Tables S2 and S3. The R^2 of the aforementioned correlations
203 for 1-OH-PRDs are larger than those for 3-OH-PRDs for both the ^{13}C and ^{1}H NMR chemical
204 shifts of the *cis* and *trans* products. For example, the correlation for ^{13}C NMR of 1-OH-PRD$_{cis}$

has a R^2 of 0.9987, which is larger than the R^2 of 0.9944 for the corresponding 3-OH-PRD*cis* correlation. These results show that better correlations between the calculated and experimental results were obtained for the stable 1-OH-PRDs than for 3-OH-PRDs in both the *cis* and *trans* configurations. Therefore, 1-OH-PRD is considered to be the actual α-acid isomerization product, not 3-OH-PRD.

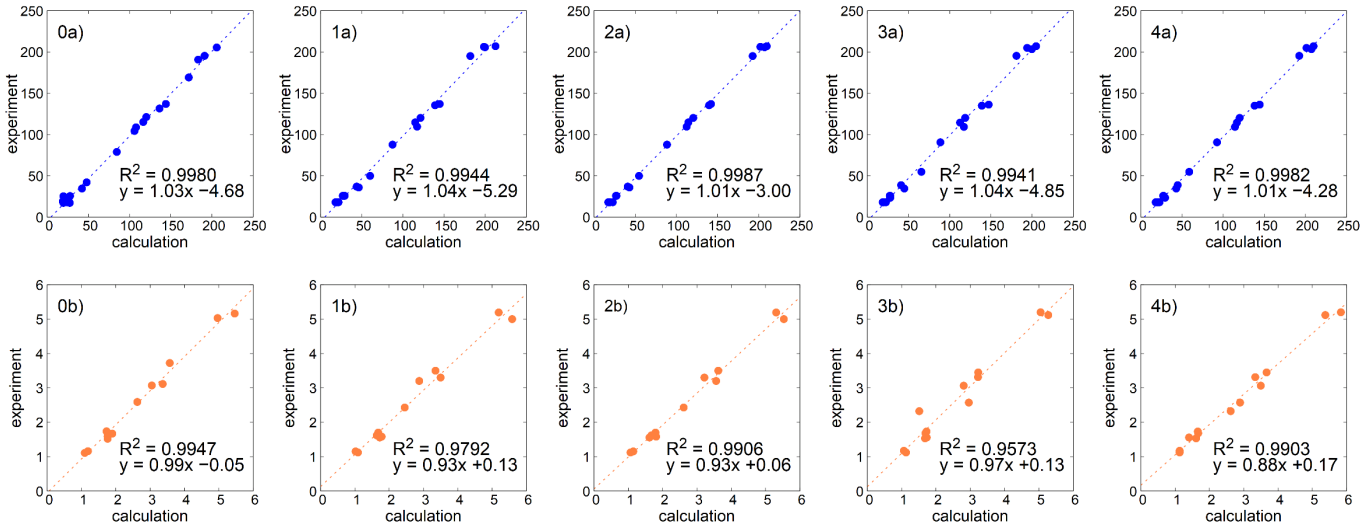

Figure 2. Correlations between experimental and calculated NMR chemical shifts for 0) cohumulone, 1) 3-OH-PRD*cis*, 2) 1-OH-PRD*cis*, 3) 3-OH-PRD*trans,* and 4) 1-OH-PRD*trans*: a) ^{13}C and b) ^{1}H

3-4. Reaction profile with Mg^{2+}

The effect of the magnesium cation on the isomerization reaction profile was investigated. The DFT calculation was used to determine the most stable structures of the Mg complexes of cohumulone and isocohumulone, which were used to propose the reaction

scheme with magnesium cation shown in Scheme S2. First, cohumulone becomes an anion by protonating a water molecule and forms the Mg-REACT complex, which includes a 6-membered ring structure with O-Mg-O coordination. Because Mg^{2+} cation is generally hexa-coordinated, 4 water molecules were additionally coordinated to Mg^{2+} cation. Next, Mg-REACT transforms into the Mg-INT intermediates, which pass through transition states, Mg-TSs, and finally generate the products, Mg-PRDs.

The reaction profile of the isomerization of cohumulone with the Mg cation calculated with the 3D-RISM-SCF method is shown in Figure 3b. The reaction profile of anionic cohumulone is included in Figure 3a for comparison.

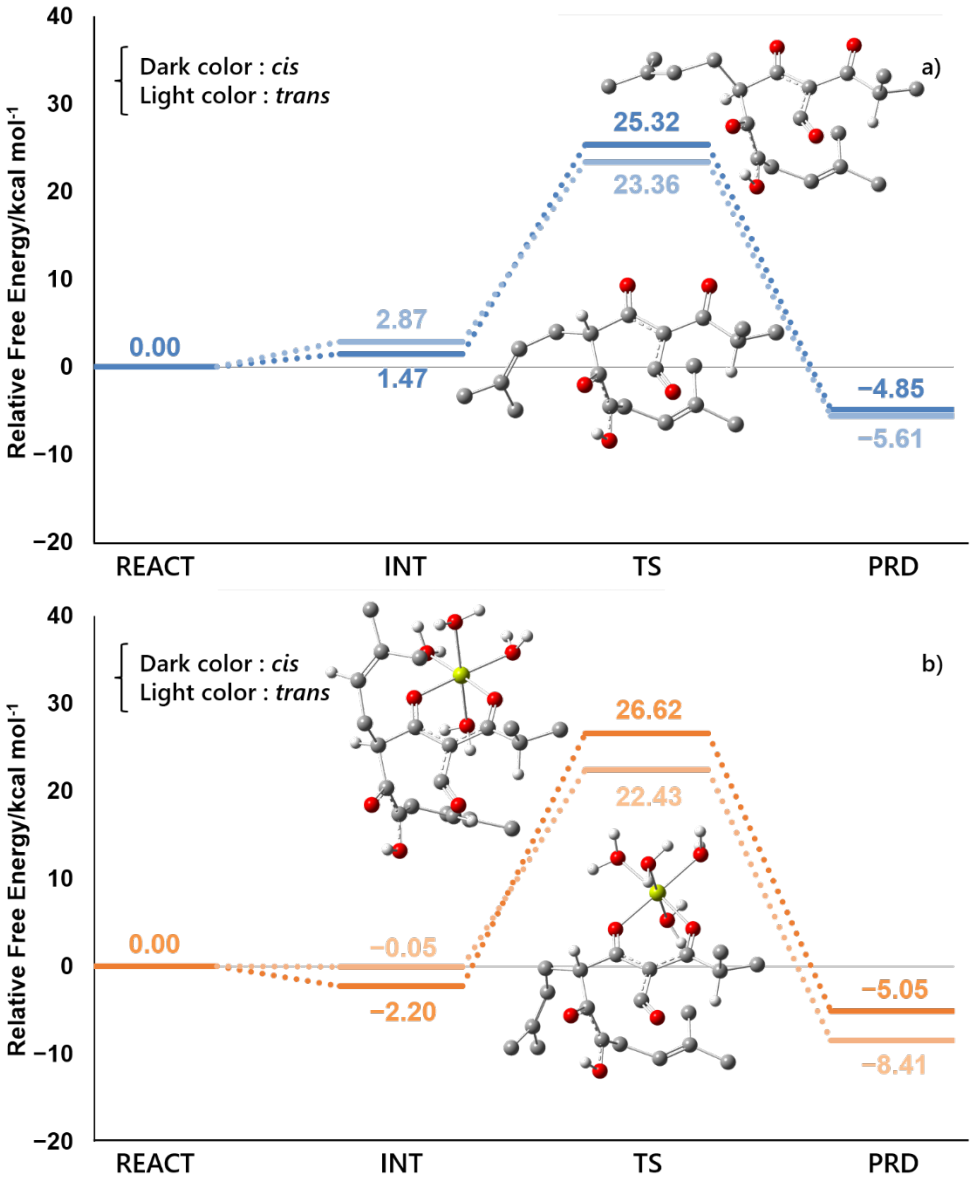

Figure 3. Isomerization reaction profiles for a) anionic cohumulone and b) Mg^{2+} complex.

Table 1 shows the activation free energy and the reaction free energy for the aforementioned isomerization reactions. The activation and reaction free energies of the Mg complex are approximately 5 kcal/mol lower than those of the neutral states. For example, the activation free energy of the Mg complex in the *trans* configuration (22.43 kcal/mol) is lower

than for anionic and neutral cohumulone (23.36 and 29.84 kcal/mol, respectively). This result is consistent with experimental results (Jaskula et al., 2010; Köller, 1969; Kostrzewa et al., 2016).

Table 1. Activation and reaction free energy differences (in kcal/mol)

	$\Delta G^{\ddagger}$		$\Delta_r G$	
	trans	*cis*	*trans*	*cis*
Mg^{2+}	22.43	26.62	–8.41	–5.05
anion	23.36	25.32	–5.61	–4.85
neutral	29.84	31.62	–0.58	–1.35

We determined the cause of the decrease in the activation free energy of the Mg complex by decomposing the activation free energy $\Delta G^{\ddagger}$ into three contributions, the structural energy in the gas phase ΔE_{gas}, the solvation free energy difference $\Delta \mu_{sol}$ and the thermal free energy difference $\Delta G_{thermal}$ between TS and REACT:

$$\Delta G^{\ddagger} = \Delta E_{gas} + \Delta \mu_{sol} + \Delta G_{thermal} \quad (2)$$

where $\Delta E_{gas} = E_{gas}(\mathrm{TS}) - E_{gas}(\mathrm{REACT})$, and $\Delta \mu_{sol}$ and $\Delta G_{thermal}$ are defined analogously. We evaluated the activation free energy differences between the Mg complexes and neutral cohumulone to compare the relative size of each contribution:

$$\Delta\Delta G^{\ddagger} = \Delta\Delta E_{gas} + \Delta\Delta \mu_{sol} + \Delta\Delta G_{thermal} \quad (3)$$

where $\Delta\Delta G^{\ddagger} = \Delta G^{\ddagger}(Mg^{2+}) - \Delta G^{\ddagger}(\mathrm{neutral})$, and $\Delta\Delta E_{gas}$, $\Delta\Delta \mu_{sol}$, and $\Delta\Delta G_{thermal}$ are defined analogously. The calculated results for the *cis* and *trans* activation free energies are shown in

Table 2. The solvation energy difference contributes considerably to the decreases in the activation free energies of –13.61 and –27.47 kcal/mol for the *cis* and *trans* configurations, respectively. This result shows that one of the major factors that stabilize the TS of Mg complexes is the large difference in the solvation free energies between REACT and the TS of Mg complexes.

Table 2. Decomposition analysis of activation free energy differences (in kcal/mol)

Mg^{2+}–neutral	$\Delta\Delta G^{\ddagger}$	$\Delta\Delta E_{gas}$	$\Delta\Delta\mu_{sol}$	$\Delta\Delta G_{thermal}$
cis	–5.00	9.39	–13.61	–0.79
trans	–7.41	20.35	–27.47	–0.30

Finally, the effect of complex formation on the absorption spectra was investigated by calculating UV-VIS absorption spectra at the TD-B3LYP-GD3(BJ)/6-31+G(d,p) level for the neutral and anionic states and the Mg^{2+}, Fe^{2+}, and Fe^{3+} complexes (Figure S2). As in the case of the Mg^{2+} complex, 4 water molecules were additionally coordinated to Fe^{2+} and Fe^{3+} complexes. In Fe^{2+} and Fe^{3+} complexes, only SMD results are shown because of the difficulty of calculating the higher excited states using 3D-RISM-SCF. It is noted that there is no qualitative difference between 3D-RISM-SCF and SMD results in the lower excited states. Considering the long-wavelength tail, the spectrum of the Mg^{2+} complex (Figure S2c) is similar to those of the neutral and anionic states (Figures S2a and S2b). In these cases, no peak is found at >400 nm, and the

longest-wavelength (lowest-energy) peak corresponding to the π-π* excitation is located at approximately 350 nm. By contrast, the spectra of the Fe^{2+} and Fe^{3+} complexes (Figures S2d and S2e) are very different from that of REACT. The spectra of these complexes exhibit several peaks at >400 nm and long-wavelength tails. The complexes have an empty low-energy *d*-type molecular orbital that enables ligand-to-metal charge transfer (LMCT) transitions to proceed at a low excitation energy. These results are consistent with experimental results (Wietstock et al., 2016) and indicate that it is difficult to determine the complexation of Mg^{2+} cation with α-acids using UV-VIS spectra alone.

5. Conclusions

In summary, the mechanism for the isomerization of cohumulone, the hydroxyl proton position of isocohumulone, and the effect of Mg^{2+} addition on isomerization were theoretically investigated. The calculated reaction profile and the activation free energy difference between *cis* and *trans* configurations are consistent with experimental results. The activation free energy difference between the *cis* and *trans* configurations is attributed to the solvation energy. An analysis of the calculated reaction profile and the NMR spectra showed that 1-OH-PRD is the actual isomerization product, not 3-OH-PRD. The isomerization reaction profile for cohumulone with Mg^{2+} demonstrated that Mg^{2+} increases iso-α-acids yields and accelerates isomerization, which is in good agreement with experimental results. The solvent effect of water contributes considerably to the decrease in the activation free energy of the isomerization reaction with Mg^{2+}. Similar spectra were obtained for the Mg^{2+} complex and

cohumulone, showing that it is difficult to determine complexation using UV-VIS spectra alone.

Declaration of Competing Interests

The authors declare no competing financial interest.

Acknowledgments

This work was supported by JSPS KAKENHI Grant Numbers JP16KT0165, JP17K05757, JP18H04657, JP20H04813, and JP20H05839. The computations were performed in part at the Research Center for Computational Science, Okazaki, Japan.

Appendix A. Supplementary data

Supplementary data associated with this article can be found, in the online version, at http://dx.doi.org.

References

Askew, H. O. (1964). Changes in Hop α Acids Concentrations on Heating in Aqueous Solutions and Unhopped Worts. *Journal of the Institute of Brewing*, *70*(6), 503–513. https://doi.org/10.1002/j.2050-0416.1964.tb06356.x

307 Beglov, D., & Roux, B. (1997). An integral equation to describe the solvation of polar
308 molecules in liquid water. *Journal of Physical Chemistry B*, *101*(39), 7821–7826.
309 https://doi.org/10.1021/jp971083h
310 Berendsen, H. J. C., Postma, J. P. M., van Gunsteren, W. F., & Hermans, J. (1981). Interaction
311 Models for Water in Relation to Protein Hydration. In *Intermolecular Forces* (Vol. 3,
312 Issue September, pp. 331–342). https://doi.org/10.1007/978-94-015-7658-1_21
313 De Keukeleire, D., & Verzele, M. (1971). The absolute configuration of the isohumulones and
314 the humulinic acids. *Tetrahedron*, *27*(20), 4939–4945. https://doi.org/10.1016/S0040-
315 4020(01)98199-2

316 De Keukeleire, Denis. (2000). Fundamentals of beer and hop chemistry. *Química Nova*,
317 *23*(1), 108–112. https://doi.org/10.1590/S0100-40422000000100019

318 Delyser, D. Y., & Kasper, W. J. (1994). Hopped Beer: The Case For Cultivation. *Economic*
319 *Botany*, *48*(2), 166–170. https://doi.org/10.1007/BF02908210

320 Ditchfield, R. (1974). Self-consistent perturbation theory of diamagnetism I. A gauge-
321 invariant LCAO method for N.M.R. Chemical shifts. *Molecular Physics*, *27*(4), 789–807.
322 https://doi.org/10.1080/00268977400100711

323 Frisch, M. J., Trucks, G. W., Schlegel, H. B., Scuseria, G. E., Robb, M. A., Cheeseman, J. R.,
324 Scalmani, G., Barone, V., Petersson, G. A., Nakatsuji, H., Li, X., Caricato, M., Marenich,
325 A. V., Bloino, J., Janesko, B. G., Gomperts, R., Mennucci, B., Hratchian, H. P., Ortiz, J.

V., Izmaylov, A. F., Sonnenberg, J. L., Williams-Young, D., Ding, F., Lipparini, F., Egidi, F., Goings, J., Peng, B., Petrone, A., Henderson, T., Ranasinghe, D., Zakrzewski, V. G., Gao, J., Rega, N., Zheng, G., Liang, W., Hada, M., Ehara, M., Toyota, K., Fukuda, R., Hasegawa, J., Ishida, M., Nakajima, T., Honda, Y., Kitao, O., Nakai, H., Vreven, T., Throssell, K., Montgomery, J. A., Jr., Peralta, J. E., Ogliaro, F., Bearpark, M. J., Heyd, J. J., Brothers, E. N., Kudin, K. N., Staroverov, V. N., Keith, T. A., Kobayashi, R., Normand, J., Raghavachari, K., Rendell, A. P., Burant, J. C., Iyengar, S. S., Tomasi, J., Cossi, M., Millam, J. M., Klene, M., Adamo, C., Cammi, R., Ochterski, J. W., Martin, R. L., Morokuma, K., Farkas, O., Foresman, J. B., Fox, D. J. (2016). Gaussian 16, Revision A.03, Gaussian, Inc., Wallingford CT.

Grimme, S., Ehrlich, S., & Goerigk, L. (2011). Effect of the damping function in dispersion corrected density functional theory. *Journal of Computational Chemistry*, *32*(7), 1456–1465. https://doi.org/10.1002/jcc.21759

Hoek, A. C., Hermans-Lokkerbol, A. C. J., & Verpoorte, R. (2001). An improved NMR method for the quantification of α-acids in hops and hop products. *Phytochemical Analysis*, *12*(1), 53–57. https://doi.org/10.1002/1099-1565(200101/02)12:1<53::AID-PCA550>3.0.CO;2-E

Jaskula-Goiris, B., Aerts, G., & De Cooman, L. (2010). Hop α-acids isomerisation and utilisation: An experimental review. *Cerevisia*, *35*(3), 57–70. https://doi.org/10.1016/j.cervis.2010.09.004

346 Jaskula, B., Aerts, G., & De Cooman, L. (2010). Potential impact of medium characteristics on
347 the isomerisation of hop α-acids in wort and buffer model systems. *Food Chemistry*,
348 *123*(4), 1219–1226. https://doi.org/10.1016/j.foodchem.2010.05.090

349 Jaskula, B., Kafarski, P., Aerts, G., & De Cooman, L. (2008). A kinetic study on the
350 isomerization of hop α-acids. *Journal of Agricultural and Food Chemistry*, *56*(15), 6408–
351 6415. https://doi.org/10.1021/jf8004965

352 Khatib, A., Wilson, E. G., Kim, H. K., Supardi, M., Choi, Y. H., & Verpoorte, R. (2007). NMR
353 assignment of iso-α-acids from isomerised extracts of Humulus lupulus L. cones.
354 *Phytochemical Analysis*, *18*(5), 371–377. https://doi.org/10.1002/pca.991

355 Köller, H. (1969). Magnesium Ion Catalysed Isomerization of Humulone: A New Route to
356 Pure Isohumulones. *Journal of the Institute of Brewing*, *75*(2), 175–179.
357 https://doi.org/10.1002/j.2050-0416.1969.tb03197.x

358 Kostrzewa, D., Dobrzyńska–Inger, A., Rój, E., Grzęda, K., & Kozłowski, K. (2016).
359 Isomerization of hop extract α-acids. *Journal of the Institute of Brewing*, *122*(3), 493–
360 499. https://doi.org/10.1002/jib.349

361 Kovalenko, A., & Hirata, F. (1998). Three-dimensional density profiles of water in contact
362 with a solute of arbitrary shape: A RISM approach. *Chemical Physics Letters*, *290*(1–3),
363 237–244. https://doi.org/10.1016/S0009-2614(98)00471-0

364 Lam, Y. H., & Houk, K. N. (2014). How cinchona alkaloid-derived primary amines control
365 asymmetric electrophilic fluorination of cyclic ketones. *Journal of the American*
366 *Chemical Society*, *136*(27), 9556–9559. https://doi.org/10.1021/ja504714m
367 Lance, D. G., White, A. W., Hildebrand, R. P., & Clarke, B. J. (1975). the Effect of Heat on
368 Metal Humulate and Isohumulate Salts. *Journal of the Institute of Brewing*, *81*(5), 364–
369 367. https://doi.org/10.1002/j.2050-0416.1975.tb06406.x

370 Malowicki, M. G., & Shellhammer, T. H. (2005). Isomerization and degradation kinetics of
371 hop (Humulus lupulus) acids in a model wort-boiling system. *Journal of Agricultural*
372 *and Food Chemistry*, *53*(11), 4434–4439. https://doi.org/10.1021/jf0481296

373 Marenich, A. V., Cramer, C. J., & Truhlar, D. G. (2009). Universal solvation model based on
374 solute electron density and on a continuum model of the solvent defined by the bulk
375 dielectric constant and atomic surface tensions. *Journal of Physical Chemistry B*,
376 *113*(18), 6378–6396. https://doi.org/10.1021/jp810292n

377 Milenković, D. A., Dimić, D. S., Avdović, E. H., Amić, A. D., Dimitrić Marković, J. M., &
378 Marković, Z. S. (2020). Advanced oxidation process of coumarins by hydroxyl radical:
379 Towards the new mechanism leading to less toxic products. *Chemical Engineering*
380 *Journal*, *395*(April), 124971. https://doi.org/10.1016/j.cej.2020.124971
381 Milenković, D., Đorović, J., Petrović, V., Avdović, E., & Marković, Z. (2018). Hydrogen atom
382 transfer versus proton coupled electron transfer mechanism of gallic acid with different

383 peroxy radicals. *Reaction Kinetics, Mechanisms and Catalysis*, *123*(1), 215–230.
384 https://doi.org/10.1007/s11144-017-1286-8
385 Ochterski, J. W., & Ph, D. (2000). Thermochemistry in Gaussian. *Gaussian Inc Pittsburgh*
386 *PA*, *264*(1), 1–19. https://doi.org/10.1016/j.ijms.2007.04.005
387 Ocvirk, M., & Košir, I. J. (2020). Dynamics of isomerization of hop alpha-acids and transition
388 of hop essential oil components in beer. *Acta Chimica Slovenica*, *67*(3), 720–728.
389 https://doi.org/10.17344/acsi.2020.5394
390 Petrov, A. S., Bowman, J. C., Harvey, S. C., & Williams, L. D. (2011). Bidentate RNA-
391 magnesium clamps: On the origin of the special role of magnesium in RNA folding.
392 *RNA*, *17*(2), 291–297. https://doi.org/10.1261/rna.2390311
393 Ribeiro, R. F., Marenich, A. V., Cramer, C. J., & Truhlar, D. G. (2011). Use of solution-phase
394 vibrational frequencies in continuum models for the free energy of solvation. *Journal of*
395 *Physical Chemistry B*, *115*(49), 14556–14562. https://doi.org/10.1021/jp205508z
396 Sato, H., Kovalenko, A., & Hirata, F. (2000). Self-consistent field, ab initio molecular orbital
397 and three-dimensional reference interaction site model study for solvation effect on
398 carbon monoxide in aqueous solution. *The Journal of Chemical Physics*, *112*(21), 9463–
399 9468. https://doi.org/10.1063/1.481564
400 Schmidt, M. W., Baldridge, K. K., Boatz, J. A., Elbert, S. T., Gordon, M. S., Jensen, J. H.,
401 Koseki, S., Matsunaga, N., Nguyen, K. A., Su, S., Windus, T. L., Dupuis, M., &
402 Montgomery, J. A. (1993). General atomic and molecular electronic structure system.

403 *Journal of Computational Chemistry*, *14*(11), 1347–1363.
404 https://doi.org/10.1002/jcc.540141112

405 Schönberger, C., & Kostelecky, T. (2011). 125th anniversary review: The role of hops in
406 brewing. *Journal of the Institute of Brewing*, *117*(3), 259–267.
407 https://doi.org/10.1002/j.2050-0416.2011.tb00471.x

408 Steenackers, B., De Cooman, L., & De Vos, D. (2015). Chemical transformations of
409 characteristic hop secondary metabolites in relation to beer properties and the brewing
410 process: A review. *Food Chemistry*, *172*, 742–756.
411 https://doi.org/10.1016/j.foodchem.2014.09.139

412 Tošović, J., Marković, S., Dimitrić Marković, J. M., Mojović, M., & Milenković, D. (2017).
413 Antioxidative mechanisms in chlorogenic acid. *Food Chemistry*, *237*, 390–398.
414 https://doi.org/10.1016/j.foodchem.2017.05.080

415 Urban, J., Dahlberg, C. J., Carroll, B. J., & Kaminsky, W. (2013). Absolute configuration of
416 beer's bitter compounds. *Angewandte Chemie - International Edition*, *52*(5), 1553–1555.
417 https://doi.org/10.1002/anie.201208450

418 Verzele, M., & van Boven, M. (1971). The Isomerization Mechanism of Humulone. *Bulletin*
419 *Des Sociétés Chimiques Belges*, *80*(5–6), 677–682.
420 https://doi.org/10.1002/bscb.19710800538

421 Wang, J., Wolf, R. M., Caldwell, J. W., Kollman, P. A., & Case, D. A. (2004). Development
422 and testing of a general Amber force field. *Journal of Computational Chemistry*, *25*(9),
423 1157–1174. https://doi.org/10.1002/jcc.20035
424 Wietstock, P. C., Kunz, T., Pereira, F., & Methner, F. J. (2016). Metal chelation behavior of
425 hop acids in buffered model systems. *BrewingScience*, *69*(9–10), 56–63.
426 Yoshida, N., & Hirata, F. (2006). A new method to determine electrostatic potential around a
427 macromolecule in solution from molecular wave functions. *Journal of Computational*
428 *Chemistry*, *27*(4), 453–462. https://doi.org/10.1002/jcc.20356
429 Yoshida, N., Kiyota, Y., & Hirata, F. (2011). The electronic-structure theory of a large-
430 molecular system in solution: Application to the intercalation of proflavine with
431 solvated DNA. *Journal of Molecular Liquids*, *159*(1), 83–92.
432 https://doi.org/10.1016/j.molliq.2010.04.019
433 Zanoli, P., & Zavatti, M. (2008). Pharmacognostic and pharmacological profile of Humulus
434 lupulus L. *Journal of Ethnopharmacology*, *116*(3), 383–396.
435 https://doi.org/10.1016/j.jep.2008.01.011

436

437 **Graphical abstract**

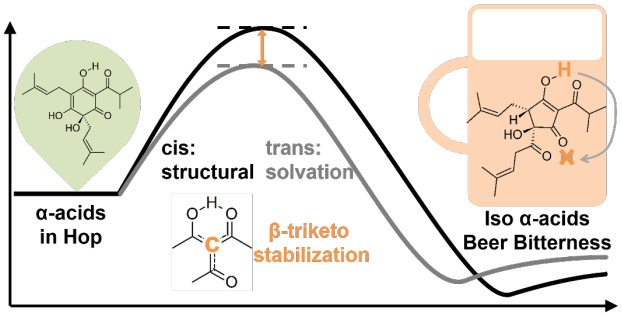

438